diagram in Fig. 8 assumes that for correct Q the output of the Q model is K times as large as its input so that for correct Q the inputs of the comparator are equal. The DC error signal V_Q resulting from the comparison is fed back to the Q model circuit to adjust the bias voltages appropriately, as well as to the filter. In these two interacting control loops, the frequency loop will converge independently of the Q control loop, but to converge on the correct value of Q, the frequency must be accurate. Hence, the two loops must operate together. The correct operation and convergence of the frequency and Q control scheme in Fig. 8 has been verified by experiments (see Schaumann et al. [3], Chapter 7, pp. 410–486) but because of the increased noise, power consumption, and chip area needed for the control circuitry, the method has not found its way into commercial applications.

BIBLIOGRAPHY

1. G. Moschytz, *Linear Integrated Networks: Design*, Van Nostrand-Reinhold, New York, 1975.
2. P. Bowron and F. W. Stevenson, *Active Filters for Communications and Instrumentation*, McGraw-Hill, Maidenhead, UK, 1979.
3. R. Schaumann, M.S. Ghausi, and K.R. Laker, *Design of Analog Filters: Passive, Active RC and Switched Capacitor*, Prentice-Hall, Englewood Cliffs, NJ, 1990.
4. W. E. Heinlein and W. H. Holmes, *Active Filters for Integrated Circuits*, R. Oldenburg, Munich, 1974.
5. E. Christian, *LC Filters: Design, Testing and Manufacturing*, Wiley, New York, 1983.
6. D. A. Johns and K. Martin, *Analog Integrated Circuit Design*, Wiley, New York, 1997.
7. Y. Tsividis and J. A. Voorman, eds., *Integrated Continuous-Time Filters: Principles, Design and Implementations*, IEEE Press, Piscataway, NJ, 1993.
8. J. F. Parker and K. W. Current, A CMOS continuous-time bandpass filter with peak-detection-based automatic tuning, *Int. J. Electron.* **1996**(5):551–564 (1996).

CIRCULAR WAVEGUIDES[1]

CONSTANTINE A. BALANIS
Arizona State University
Tempe, Arizona
(edited by Eric Holzman
Northrop Grumman Electronic
Systems, Baltimore, Maryland)

1. INTRODUCTION

The circular waveguide is occasionally used as an alternative to the rectangular waveguide. Like other waveguides constructed from a single, enclosed conductor, the circular waveguide supports transverse electric (TE) and transverse magnetic (TM) modes. These modes have a cutoff frequency, below which electromagnetic energy is severely attenuated. Circular waveguide's round cross section makes it easy to machine, and it is often used to feed conical horns. Further, the TE_{0n} modes of circular waveguide have very low attenuation. A disadvantage of circular waveguide is its limited dominant mode bandwidth, which, compared to rectangular waveguide's maximum bandwidth of 2–1, is only 1.3. In addition, the polarization of the dominant mode is arbitrary, so that discontinuities can easily excite unwanted cross-polarized components.

In this article, the electromagnetic features of the circular waveguide are summarized, including the transverse and longitudinal fields, the cutoff frequencies, the propagation and attenuation constants, and the wave impedances of all transverse electric and transverse magnetic modes.

2. TRANSVERSE ELECTRIC (TE^z) MODES

The transverse electric to z (TE^z) modes can be derived by letting the vector potential $\mathbf{A}$ and $\mathbf{F}$ be equal to

$$\mathbf{A} = 0 \tag{1a}$$

$$\mathbf{F} = \hat{a}_z F_z(\rho, \phi, z) \tag{1b}$$

The vector potential $\mathbf{F}$ must satisfy the vector wave equation, which reduces the $\mathbf{F}$ of (1b) to

$$\nabla^2 F_z(\rho, \phi, z) + \beta^2 F_z(\rho, \phi, z) = 0 \tag{2}$$

When expanded in cylindrical coordinates, (2) reduces to

$$\frac{\partial^2 F_z}{\partial \rho^2} + \frac{1}{\rho}\frac{\partial F_z}{\partial \rho} + \frac{1}{\rho^2}\frac{\partial^2 F_z}{\partial \phi^2} + \frac{\partial^2 F_z}{\partial z^2} + \beta^2 F_z = 0 \tag{3}$$

whose solution for the geometry of Fig. 1 is of the form

$$\begin{aligned} F_z(\rho, \phi, z) = {} & [A_1 J_m(\beta_\rho \rho) + B_1 Y_m(\beta_\rho \rho)] \\ & \times [C_2 \cos(m\phi) + D_2 \sin(m\phi)] \\ & \times [A_3 e^{-j\beta_z z} + B_3 e^{+j\beta_z z}] \end{aligned} \tag{4a}$$

where

$$\beta_\rho^2 + \beta_z^2 = \beta^2 \tag{4b}$$

The constants A_1, B_1, C_2, D_2, A_3, B_3, m, β_ρ, and β_z can be found using the boundary conditions of

$$E_\phi(\rho = a, \phi, z) = 0 \tag{5a}$$

The fields must be finite everywhere (5b)

The fields must repeat every 2π radians in ϕ (5c)

[1]This article is derived from material in *Advanced Engineering Electromagnetics*, by Constantine Balanis, Wiley, New York, 1989, Sect. 9.2.

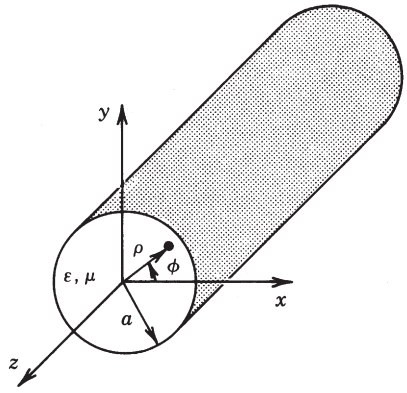

Figure 1. Cylindrical waveguide of circular cross section.

According to (5b), $B_1 = 0$ since $Y_m(\rho = 0) = \infty$. In addition, according to (5c)

$$m = 0, 1, 2, 3, \ldots \tag{6}$$

Consider waves that propagate only in the $+z$ direction. Then (4) reduces to

$$F_z^+(\rho, \phi, z) = A_{mn} J_m(\beta_\rho \rho)[C_2 \cos(m\phi) + D_2 \sin(m\phi)]e^{-j\beta_z z} \tag{7}$$

From Eq. (7), the electric field component of E_ϕ^+ can be written as

$$E_\phi^+ = \frac{1}{\varepsilon}\frac{\partial F_z^+}{\partial \rho} = \beta_\rho \frac{A_{mn}}{\varepsilon} J_m'(\beta_\rho \rho)[C_2 \cos(m\phi) + D_2 \sin(m\phi)]e^{-j\beta_z z} \tag{8a}$$

where

$$' = \frac{\partial}{\partial(\beta_\rho \rho)} \tag{8b}$$

Applying the boundary condition of (5a) in (8a), we then have that

$$E_\phi^+(\rho = a, \phi, z) = \beta_\rho \frac{A_{mn}}{\varepsilon} J_m'(\beta_\rho a)[C_2 \cos(m\phi) + D_2 \sin(m\phi)]e^{-j\beta_z z} = 0 \tag{9}$$

which is satisfied only provided that

$$J_m'(\beta_\rho a) = 0 \Rightarrow \beta_\rho a = \chi_{mn}' \Rightarrow \beta_\rho = \frac{\chi_{mn}'}{a} \tag{10}$$

In (10) χ_{mn}' represents the nth zero ($n = 1, 2, 3, \ldots$) of the derivative of the Bessel function J_m of the first kind of order $m (m = 0, 1, 2, 3, \ldots)$. An abbreviated list of the zeros χ_{mn}' of the derivative J_m' of the Bessel function J_m is found in Table 1. The smallest value of χ_{mn}' is 1.8412 ($m = 1$, $n = 1$).

Using (4b) and (10), β_z of the mn mode can be written as

$$(\beta_z)_{mn} = \begin{cases} \sqrt{\beta^2 - \beta_\rho^2} = \sqrt{\beta^2 - \left(\frac{\chi_{mn}'}{a}\right)^2} \\ \text{when } \beta > \beta_\rho = \dfrac{\chi_{mn}'}{a} \end{cases} \tag{11a}$$

$$(\beta_z)_{mn} = \begin{cases} 0 \quad \text{when } \beta = \beta_c = \beta_\rho = \dfrac{\chi_{mn}'}{a} \end{cases} \tag{11b}$$

$$(\beta_z)_{mn} = \begin{cases} -j\sqrt{\beta_\rho^2 - \beta^2} = -j\sqrt{\left(\frac{\chi_{mn}'}{a}\right)^2 - \beta^2} \\ \text{when } \beta < \beta_\rho = \dfrac{\chi_{mn}'}{a} \end{cases} \tag{11c}$$

Cutoff is defined when $(\beta_z)_{mn} = 0$. Thus, according to (11b)

$$\beta_c = \omega_c \sqrt{\mu\varepsilon} = 2\pi f_c \sqrt{\mu\varepsilon} = \beta_\rho = \frac{\chi_{mn}'}{a} \tag{12a}$$

$$(f_c)_{mn} = \frac{\chi_{mn}'}{2\pi a \sqrt{\mu\varepsilon}} \tag{12b}$$

By using (12a) and (12b), we can write (11a)–(11c) as

$$(\beta_z)_{mn} = \begin{cases} \sqrt{\beta^2 - \beta_\rho^2} = \beta\sqrt{1 - \left(\frac{\beta_\rho}{\beta}\right)^2} = \beta\sqrt{1 - \left(\frac{\beta_c}{\beta}\right)^2} \\ = \beta\sqrt{1 - \left(\frac{\chi_{mn}'}{\beta a}\right)^2} = \beta\sqrt{1 - \left(\frac{f_c}{f}\right)^2} \\ \text{when } f > f_c = (f_c)_{mn} \end{cases} \tag{13a}$$

$$(\beta_z)_{mn} = \{ 0 \quad \text{when } f = f_c = (f_c)_{mn} \tag{13b}$$

Table 1. Zeros χ'_{mn} of Derivative $J'_m(\chi'_{mn}) = 0$ ($n = 1,2,3,\ldots$) of Bessel Function $J_m(x)$

	$m=0$	$m=1$	$m=2$	$M=3$	$m=4$	$m=5$	$m=6$	$m=7$	$m=8$	$m=9$	$m=10$	$m=11$
$n=1$	3.8318	1.8412	3.0542	4.2012	5.3175	6.4155	7.5013	8.5777	9.6474	10.7114	11.7708	12.8264
$n=2$	7.0156	5.3315	6.7062	8.0153	9.2824	10.5199	11.7349	12.9324	14.1155	15.2867	16.4479	17.6003
$n=3$	10.1735	8.5363	9.9695	11.3459	12.6819	13.9872	15.2682	16.5294	17.7740	19.0046	20.2230	21.4309
$n=4$	13.3237	11.7060	13.1704	14.5859	15.9641	17.3129	18.6375	19.9419	21.2291	22.5014	23.7607	25.0085
$n=5$	16.4706	14.8636	16.3475	17.7888	19.1960	20.5755	21.9317	23.2681	24.5872	25.8913	27.1820	28.4609

$$(\beta_z)_{mn}=\begin{cases}-j\sqrt{\beta_\rho^2-\beta^2}=-j\beta\sqrt{\left(\dfrac{\beta_\rho}{\beta}\right)^2-1}=-j\beta\sqrt{\left(\dfrac{\beta_c}{\beta}\right)^2-1}\\ =-j\beta\sqrt{\left(\dfrac{\chi'_{mn}}{\beta a}\right)^2-1}=-j\beta\sqrt{\left(\dfrac{f_c}{f}\right)^2-1}\\ \text{when } f<f_c=(f_c)_{mn}\end{cases}\tag{13c}$$

The guide wavelength λ_g is defined as

$$(\lambda_g)_{mn}=\frac{2\pi}{(\beta_z)_{mn}}\tag{14a}$$

which, according to (13a) and (13b), can be written as

$$(\lambda_g)_{mn}=\begin{cases}\dfrac{2\pi}{\beta\sqrt{1-\left(\dfrac{f_c}{f}\right)^2}}=\dfrac{\lambda}{\sqrt{1-\left(\dfrac{f_c}{f}\right)^2}} & \text{when } f>f_c=(f_c)_{mn}\end{cases}\tag{14b}$$

$$(\lambda_g)_{mn}=\{\infty \text{ when } f=(f_c)_{mn}\tag{14c}$$

In (14b) λ is the wavelength of the wave in an infinite medium of the kind that exists inside the waveguide. There is no definition of the wavelength below cutoff since the wave is exponentially decaying and there is no repetition of its waveform.

According to (12b) and the values of χ'_{mn} in Table 1, the order (lower to higher cutoff frequencies) in which the TE^z_{mn} modes occur is TE^z_{11}, TE^z_{21}, TE^z_{01}, and so on. It should be noted that for a circular waveguide, the order in which the TE^z_{mn} modes occur does not change, and the bandwidth between modes is also fixed. For example, the bandwidth of the first single-mode TE^z_{11} operation is $3.042/1.8412=1.6588:1$, which is less than $2:1$. This bandwidth is fixed and cannot be varied. A change in the radius only varies, by the same amount, the absolute values of the cutoff frequencies of all the modes but does not alter their order or relative bandwidth.

The electric and magnetic field components can be written from Eq. (7) as

$$\begin{aligned}E_\rho^+&=-\frac{1}{\varepsilon\rho}\frac{\partial F_z^+}{\partial\phi}\\&=-A_{mn}\frac{m}{\varepsilon\rho}J_m(\beta_\rho\rho)[-C_2\sin(m\phi)\\&\quad+D_2\cos(m\phi)]e^{-j\beta_z z}\end{aligned}\tag{15a}$$

$$\begin{aligned}E_\phi^+&=\frac{1}{\varepsilon}\frac{\partial F_z^+}{\partial\rho}\\&=A_{mn}\frac{\beta_\rho}{\varepsilon}J'_m(\beta_\rho\rho)[C_2\cos(m\phi)\\&\quad+D_2\sin(m\phi)]e^{-j\beta_z z}\end{aligned}\tag{15b}$$

$$E_z^+=0\tag{15c}$$

$$\begin{aligned}H_\rho^+&=-j\frac{1}{\omega\mu\varepsilon}\frac{\partial^2F_z^+}{\partial\rho\partial z}\\&=-A_{mn}\frac{\beta_\rho\beta_z}{\omega\mu\varepsilon}J'_m(\beta_\rho\rho)[C_2\cos(m\phi)\\&\quad+D_2\sin(m\phi)]e^{-j\beta_z z}\end{aligned}\tag{15d}$$

$$\begin{aligned}H_\phi^+&=-j\frac{1}{\omega\mu\varepsilon}\frac{1}{\rho}\frac{\partial^2F_z^+}{\partial\phi\partial z}=-A_{mn}\frac{m\beta_z}{\omega\mu\varepsilon}\frac{1}{\rho}J_m(\beta_\rho\rho)\\&\quad\times[-C_2\sin(m\phi)+D_2\cos(m\phi)]e^{-j\beta_z z}\end{aligned}\tag{15e}$$

$$\begin{aligned}H_z^+&=-j\frac{1}{\omega\mu\varepsilon}\left(\frac{\partial^2}{\partial z^2}+\beta^2\right)F_z^+=-jA_{mn}\frac{\beta_\rho^2}{\omega\mu\varepsilon}J_m(\beta_\rho\rho)\\&\quad\times[C_2\cos(m\phi)+D_2\sin(m\phi)]e^{-j\beta_z z}\end{aligned}\tag{15f}$$

where

$$'=\frac{\partial}{\partial(\beta_\rho\rho)}\tag{15g}$$

By using (15a)–(15f), the wave impedance $(Z_w^{+z})^{TE}_{mn}$ of the TE^z_{mn} (H^z_{mn}) modes in the $+z$ direction can be written as

$$Z^h_{mn}=(Z_w^{+z})^{TE}_{mn}=\frac{E_\rho^+}{H_\phi^+}=-\frac{E_\phi^+}{H_\rho^+}=\frac{\omega\mu}{(\beta_z)_{mn}}\tag{16a}$$

With the aid of (13a)–(13c) the wave impedance of (16a) reduces to

$$Z^h_{mn}=(Z_w^{+z})^{TE}_{mn}=\begin{cases}\dfrac{\omega\mu}{\beta\sqrt{1-\left(\dfrac{f_c}{f}\right)^2}}=\dfrac{\sqrt{\dfrac{\mu}{\varepsilon}}}{\sqrt{1-\left(\dfrac{f_c}{f}\right)^2}}=\dfrac{\eta}{\sqrt{1-\left(\dfrac{f_c}{f}\right)^2}}\\ \text{when } f>f_c=(f_c)_{mn}\end{cases}\tag{16b}$$

$$Z^h_{mn}=(Z_w^{+z})^{TE}_{mn}=\left\{\frac{\omega\mu}{0}=\infty\quad\text{when } f=f_c=(f_c)_{mn}\right.\tag{16c}$$

$$Z^h_{mn}=(Z_w^{+z})^{TE}_{mn}=\begin{cases}\dfrac{\omega\mu}{-j\beta\sqrt{\left(\dfrac{f_c}{f}\right)^2-1}}=+j\dfrac{\sqrt{\dfrac{\mu}{\varepsilon}}}{\sqrt{\left(\dfrac{f_c}{f}\right)^2-1}}=+j\dfrac{\eta}{\sqrt{\left(\dfrac{f_c}{f}\right)^2-1}}\\ \text{when } f<f_c=(f_c)_{mn}\end{cases}\tag{16d}$$

By examining through (16b)–(16d), we can make the following statements about the impedance.

1. Above cutoff it is real and greater than the intrinsic impedance of the medium inside the waveguide.
2. At cutoff it is infinity.

3. Below cutoff it is imaginary and inductive. This indicates that the waveguide below cutoff behaves as an inductor that is an energy storage element.

3. TRANSVERSE MAGNETIC (TM^Z) MODES

The transverse magnetic to z (TM^z) modes can be derived in a similar manner as the TE^z modes of Section 2 by letting

$$\mathbf{A} = \hat{a}_z A_z(\rho, \phi, z) \tag{17a}$$

$$\mathbf{F} = 0 \tag{17b}$$

The vector potential $\mathbf{A}$ must satisfy the vector wave equation, which reduces for the $\mathbf{A}$ of (17a) to

$$\nabla^2 A_z(\rho, \phi, z) + \beta^2 A_z(\rho, \phi, z) = 0 \tag{18}$$

The solution of (18) is obtained in a manner similar to that of (2), as given by (4), and it can be written as

$$\begin{aligned} A_z(\rho, \phi, z) = {} & [A_1 J_m(\beta_\rho \rho) + B_1 Y_m(\beta_\rho \rho)] \\ & \times [C_2 \cos(m\phi) + D_2 \sin(m\phi)] \\ & \times [A_3 e^{-j\beta_z z} + B_3 e^{+j\beta_z z}] \end{aligned} \tag{19a}$$

with

$$\beta_\rho^2 + \beta_z^2 = \beta^2 \tag{19b}$$

The constants A_1, B_1, C_2, D_2, A_3, B_3, m, β_ρ, and β_z can be found using the boundary conditions of

$$E_\phi(\rho = a, \phi, z) = 0 \tag{20a}$$

or

$$E_z = (\rho = a, \phi, z) = 0 \tag{20b}$$

The fields must be finite everywhere (20c)

The fields must repeat every 2π radians in ϕ (20d)

According to (20c), $B_1 = 0$ since $Y_m(\rho = 0) = \infty$. In addition, according to (20d),

$$m = 0, 1, 2, 3, \ldots \tag{21}$$

Considering waves that propagate only in the $+z$ direction, (19a) then reduces to

$$\begin{aligned} A_z^+(\rho, \phi, z) = {} & B_{mn} J_m(\beta_\rho \rho)[C_2 \cos(m\phi) \\ & + D_2 \sin(m\phi)] e^{-j\beta_z z} \end{aligned} \tag{22}$$

The eigenvalues of β_ρ can be obtained by applying either (20a) or (20b).

From Eq. (22), we can write the electric field component E_z^+ as

$$\begin{aligned} E_z^+ &= -j \frac{1}{\omega\mu\varepsilon} \left(\frac{\partial^2}{\partial z^2} + \beta^2 \right) A_z^+ \\ &= -jB_{mn} \frac{\beta_\rho^2}{\omega\mu\varepsilon} J_m(\beta_\rho \rho)[C_2 \cos(m\phi) \\ &\quad + D_2 \sin(m\phi)] e^{-j\beta_z z} \end{aligned} \tag{23}$$

Application of the boundary condition of (20b) using (23) gives

$$\begin{aligned} E_z^+(\rho = a, \phi, z) = {} & -jB_{mn} \frac{\beta_\rho^2}{\omega\mu\varepsilon} J_m(\beta_\rho a) \\ & \times [C_2 \cos(m\phi) + D_2 \sin(m\phi)] e^{-j\beta_z z} = 0 \end{aligned} \tag{24}$$

which is satisfied only provided that

$$J_m(\beta_\rho a) = 0 \Rightarrow \beta_\rho a = \chi_{mn} \Rightarrow \beta_\rho = \frac{\chi_{mn}}{a} \tag{25}$$

In (25) χ_{mn} represents the nth zero ($n = 1, 2, 3, \ldots$) of the Bessel function J_m of the first kind of order m ($m = 0, 1, 2, 3, \ldots$). An abbreviated list of the zeros χ_{mn} of the Bessel function J_m is found in Table 2. The smallest value of χ_{mn} is 2.4049 ($m = 0$, $n = 1$).

By using (19b) and (25), β_z can be written as

$$(\beta_z)_{mn} = \begin{cases} \sqrt{\beta^2 - \beta_\rho^2} = \sqrt{\beta^2 - \left(\frac{\chi_{mn}}{a}\right)^2} \\ \text{when } \beta > \beta_\rho = \dfrac{\chi_{mn}}{a} \end{cases} \tag{26a}$$

Table 2. Zeros χ_{mn} of $J_m(\chi_{mn}) = 0$ ($n = 1, 2, 3, \ldots$) of Bessel function $J_m(x)$

	$m=0$	$m=1$	$m=2$	$M=3$	$m=4$	$m=5$	$m=6$	$m=7$	$m=8$	$m=9$	$m=10$	$m=11$
$n=1$	2.4049	3.8318	5.1357	6.3802	7.5884	8.7715	9.9361	11.0864	12.2251	13.3543	14.4755	12.8264
$n=2$	5.5201	7.1056	8.4173	9.7610	11.0647	12.3386	13.5893	14.8213	16.0378	17.2412	18.4335	19.6160
$n=3$	8.6537	10.1735	11.6199	13.0152	14.3726	15.7002	17.0038	18.2876	19.5545	20.8071	22.0470	23.2759
$n=4$	11.7915	13.3237	14.7960	16.2235	17.6160	18.9801	20.3208	21.6415	22.9452	24.2339	25.5095	26.7733
$n=5$	14.9309	16.4706	17.9598	19.4094	20.8269	22.2178	23.5861	24.9349	26.2668	27.5838	28.8874	80.1791

$$(\beta_z)_{mn} = \begin{cases} 0 & \text{when } \beta = \beta_c = \beta_\rho = \dfrac{\chi_{mn}}{a} \end{cases} \tag{26b}$$

$$(\beta_z)_{mn} = \begin{cases} -j\sqrt{\beta_\rho^2 - \beta^2} = -j\sqrt{\left(\dfrac{\chi_{mn}}{a}\right)^2 - \beta^2} \\ \text{when } \beta < \beta_\rho = \dfrac{\chi_{mn}}{a} \end{cases} \tag{26c}$$

By following the same procedure as for the TE^z modes, we can write the expressions for the cutoff frequencies $(f_c)_{mn}$, propagation constant $(\beta_z)_{mn}$, and guide wavelength $(\lambda_g)_{mn}$ as

$$(f_c)_{mn} = \frac{\chi_{mn}}{2\pi a\sqrt{\mu\varepsilon}} \tag{27}$$

$$(\beta_z)_{mn} = \begin{cases} \sqrt{\beta^2 - \beta_\rho^2} = \beta\sqrt{1 - \left(\dfrac{\beta_\rho}{\beta}\right)^2} = \beta\sqrt{1 - \left(\dfrac{\beta_c}{\beta}\right)^2} \\ = \beta\sqrt{1 - \left(\dfrac{\chi_{mn}}{\beta a}\right)^2} = \beta\sqrt{1 - \left(\dfrac{f_c}{f}\right)^2} \\ \text{when } f > f_c = (f_c)_{mn} \end{cases} \tag{28a}$$

$$(\beta_z)_{mn} = \{ 0 \quad \text{when } f = f_c = (f_c)_{mn} \tag{28b}$$

$$(\beta_z)_{mn} = \begin{cases} -j\sqrt{\beta_\rho^2 - \beta^2} = -j\beta\sqrt{\left(\dfrac{\beta_\rho}{\beta}\right)^2 - 1} = -j\beta\sqrt{\left(\dfrac{\beta_c}{\beta}\right)^2 - 1} \\ = -j\beta\sqrt{\left(\dfrac{\chi_{mn}}{\beta a}\right)^2 - 1} = -j\beta\sqrt{\left(\dfrac{f_c}{f}\right)^2 - 1} \\ \text{when } f < f_c = (f_c)_{mn} \end{cases} \tag{28c}$$

$$(\lambda_g)_{mn} = \begin{cases} \dfrac{2\pi}{\beta\sqrt{1 - \left(\dfrac{f_c}{f}\right)^2}} = \dfrac{\lambda}{\sqrt{1 - \left(\dfrac{f_c}{f}\right)^2}} & \text{when } f > f_c = (f_c)_{mn} \end{cases} \tag{29a}$$

$$(\lambda_g)_{mn} = \{\infty \quad \text{when } f = f_c = (f_c)_{mn} \tag{29b}$$

According to (27) and the values of χ_{mn} of Table 2, the order (lower to higher cutoff frequencies) in which the TM^z modes occur is TM_{01}, TM_{11}, TM_{21}, and so forth. The bandwidth of the first single-mode TM_{01}^z operation is 3.8318/2.4059 = 1.5927:1. Comparing the cutoff frequencies of the TE^z and TM^z modes, as given by (12b) and (27) along with the data of Tables 1 and 2, the order of the TE_{mn}^z and TM_{mn}^z modes is that of TE_{11} ($\chi'_{11} = 1.8412$), TM_{01}, ($\chi_{01} = 2.4049$), TE_{21} ($\chi'_{21} = 3.0542$), TE_{01} ($\chi'_{01} = 3.8318$) = TM_{11} ($\chi'_{11} = 3.8318$), TE_{31} ($\chi'_{31} = 4.2012$), and so forth. The dominant mode is TE_{11} and its bandwidth of single-mode operation is 2.4049/1.8412 = 1.3062:1. Plots of the field configurations over a cross section of the waveguide, both E and H, for the first 30 TE_{mn}^z and/or TM_{mn}^z modes are shown in Fig. 2 [1].

It is apparent that the cutoff frequencies of the TE_{0n} and TM_{1n} modes are identical; therefore they are referred to here also as *degenerate modes*.

The electric and magnetic field components can be written using (22) as

$$\begin{aligned} E_\rho^+ &= -j\frac{1}{\omega\mu\varepsilon}\frac{\partial^2 A_z^+}{\partial\rho\partial z} \\ &= -B_{mn}\frac{\beta_\rho\beta_z}{\omega\mu\varepsilon}J'_m(\beta_\rho\rho) \\ &\quad \times [C_2\cos(m\phi) + D_2\sin(m\phi)]e^{-j\beta_z z} \end{aligned} \tag{30a}$$

$$\begin{aligned} E_\phi^+ &= -j\frac{1}{\omega\mu\varepsilon}\frac{1}{\rho}\frac{\partial^2 A_z^+}{\partial\phi\partial z} \\ &= -B_{mn}\frac{m\beta_z}{\omega\mu\varepsilon\rho}J_m(\beta_\rho\rho) \\ &\quad \times [-C_2\sin(m\phi) + D_2\cos(m\phi)]e^{-j\beta_z z} \end{aligned} \tag{30b}$$

$$\begin{aligned} E_z^+ &= -j\frac{1}{\omega\mu\varepsilon}\left(\frac{\partial^2}{\partial z^2} + \beta^2\right)A_z^+ \\ &= -jB_{mn}\frac{\beta_\rho^2}{\omega\mu\varepsilon}J_m(\beta_\rho\rho) \\ &\quad \times [C_2\cos(m\phi) + D_2\sin(m\phi)]e^{-j\beta_z z} \end{aligned} \tag{30c}$$

$$H_\rho^+ = \frac{1}{\mu}\frac{1}{\rho}\frac{\partial A_z^+}{\partial\phi} = B_{mn}\frac{m}{\mu}\frac{1}{\rho}J_m(\beta_\rho\rho) \times [-C_2\sin(m\phi) + D_2\cos(m\phi)]e^{-j\beta_z z} \tag{30d}$$

$$H_\phi^+ = -\frac{1}{\mu}\frac{\partial A_z^+}{\partial\rho} = -B_{mn}\frac{\beta_\rho}{\mu}J'_m(\beta_\rho\rho) \times [C_2\cos(m\phi) + D_2\sin(m\phi)]e^{-j\beta_z z} \tag{30e}$$

$$H_z^+ = 0 \tag{30f}$$

where

$$' = \frac{\partial}{\partial(\beta_\rho\rho)} \tag{30g}$$

By using (30a)–(30f), the wave impedance in the $+z$ direction can be written as

$$(Z_w^{+z})_{mn}^{TM} = \frac{E_\rho^+}{H_\phi^+} = -\frac{E_\phi^+}{H_\rho^+} = \frac{(\beta_z)_{mn}}{\omega\varepsilon} \tag{31}$$

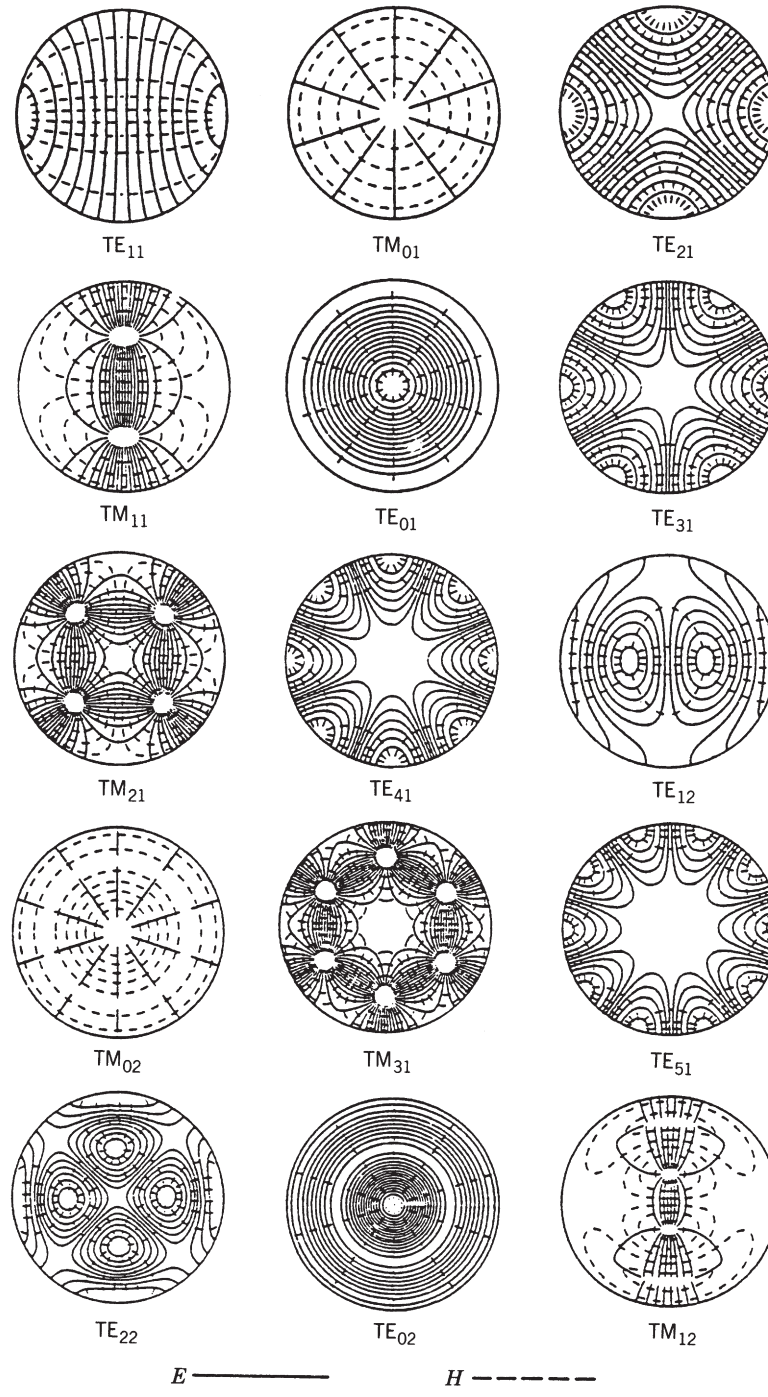

Figure 2. Field configurations of first 30 TE^z and/or TM^z modes in a circular waveguide. (*Source*: C. S. Lee, S. W. Lee, and S. L. Chuang, Plot of modal field distribution in rectangular and circular waveguides, *IEEE Trans. Microwave Theory Tech.*, © 1985, IEEE.)

With the aid of (28a)–(28c) the wave impedance of (31) reduces to

$$(Z_{\mathrm{w}}^{+z})_{mn}^{\mathrm{TM}} = \begin{cases} \dfrac{\beta\sqrt{1-\left(\dfrac{f_{\mathrm{c}}}{f}\right)^2}}{\omega\varepsilon} = \sqrt{\dfrac{\mu}{\varepsilon}}\sqrt{1-\left(\dfrac{f_{\mathrm{c}}}{f}\right)^2} = \eta\sqrt{1-\left(\dfrac{f_{\mathrm{c}}}{f}\right)^2} \\ \text{when } f > f_{\mathrm{c}} = (f_{\mathrm{c}})_{mn} \end{cases} \tag{32a}$$

$$(Z_{\mathrm{w}}^{+z})_{mn}^{\mathrm{TM}} = \left\{ \frac{0}{\omega\varepsilon} = 0 \quad \text{when } f = f_{\mathrm{c}} = (f_{\mathrm{c}})_{mn} \right. \tag{32b}$$

$$(Z_{\mathrm{w}}^{+z})_{mn}^{\mathrm{TM}} \begin{cases} \dfrac{-j\beta\sqrt{\left(\dfrac{f_{\mathrm{c}}}{f}\right)^2-1}}{\omega\varepsilon} = -j\sqrt{\dfrac{\mu}{\varepsilon}}\sqrt{\left(\dfrac{f_{\mathrm{c}}}{f}\right)^2-1} \\ \qquad = -j\eta\sqrt{\left(\dfrac{f_{\mathrm{c}}}{f}\right)^2-1} \\ \text{when } f < f_{\mathrm{c}} = (f_{\mathrm{c}})_{mn} \end{cases} \tag{32c}$$

Examining (32a)–(32c) we can make the following statements about the wave impedance for the TM^z modes.

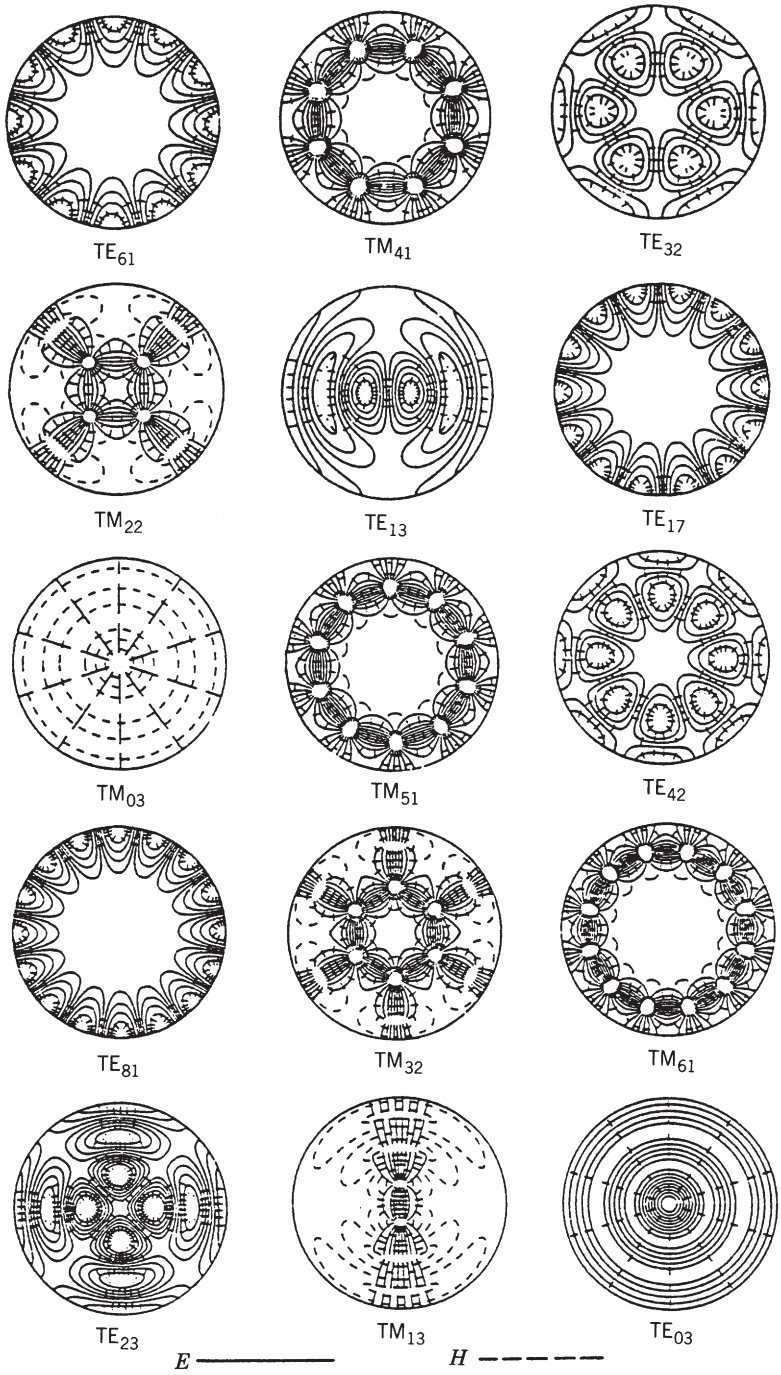

Figure 2. (Continued).

1. Above cutoff it is real and smaller than the intrinsic impedance of the medium inside the waveguide.
2. At cutoff it is zero.
3. Below cutoff it is imaginary and capacitive. This indicates that the waveguide below cutoff behaves as a capacitor that is an energy storage element.

Whenever a given mode is desired, it is necessary to design the proper feed to excite the fields within the waveguide and detect the energy associated with such modes. To maximize the energy exchange or transfer, this is accomplished by designing the feed, which is usually a probe or antenna, so that its field pattern matches that of the field configuration of the desired mode. Usually the probe is placed near the maximum of the field pattern of the desired mode; however, that position may be varied somewhat in order to achieve some desired matching in the excitation and detection systems. Shown in Fig. 3 are suggested designs to excite and/or detect the TE_{11} and TM_{01} modes in a circular waveguide, to transition between the TE_{10} of a rectangular waveguide and the TE_{11} mode of a circular waveguide, and to couple between the TE_{10} of a rectangular waveguide and TM_{01} mode of a circular waveguide.

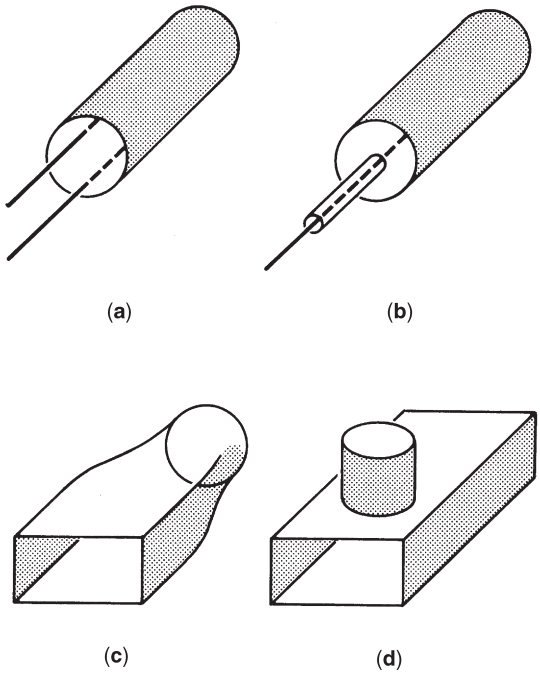

Figure 3. Excitation of TE_{mn} and TM_{mn} modes in a circular waveguide: (a) TE_{11} mode; (b) TM_{01} mode; (c) TE_{10} (rectangular)–TE_{11} (circular); (d) TE_{10} (rectangular)–TM_{01} (circular).

4. ATTENUATION FROM OHMIC LOSSES

It has been shown that the attenuation coefficients of the TE_{0n} ($n = 1,2,\ldots$) modes in a circular waveguide monotonically decrease as a function of frequency [2,3]. This is a very desirable characteristic, and because of this the excitation, propagation, and detection of TE_{0n} modes in a circular waveguide have received considerable attention. The attenuation coefficient for the TE^z_{mn} and TM^z_{mn} modes inside a circular waveguide are given, respectively, by

$$\text{TE}^z_{mn}$$

$$(\alpha_c)^{\text{TE}^z}_{mn} = \frac{R_s}{a\eta\sqrt{1-\left(\dfrac{f_c}{f}\right)^2}} \times \left[\left(\frac{f_c}{f}\right)^2 + \frac{m^2}{(\chi'_{mn})^2 - m^2}\right] \text{Np/m} \tag{33a}$$

$$\text{TM}^z_{mn}$$

$$(\alpha_c)^{\text{TM}^z}_{mn} = \frac{R_s}{a\eta}\frac{1}{\sqrt{1-\left(\dfrac{f_c}{f}\right)^2}} \text{Np/m} \tag{33b}$$

where

$$R_s = \sqrt{\frac{\omega\mu}{2\sigma}} \tag{34}$$

Plots of the attenuation coeficient versus the normalized frequency f/f_c, where f_c is the cutoff frequency of the dominant TE_{11} mode, are shown for six modes in Fig. 4a and b for waveguide radii of 1.5 and 3 cm, respectively. Within the waveguide is free space and its walls are made of copper ($\sigma = 5.7 \times 10^7$ S/m).

It is evident from the results of the preceding example that as f_c/f becomes smaller the attenuation coefficient decreases monotonically (as shown in Fig. 4), which is a desirable characteristic. It should be noted that similar monotonically decreasing variations in the attenuation coefficient are evident in all TE_{0n} modes ($n = 1,2,3,\ldots$). According to (15a)–(15f), the only tangential magnetic field component to the conducting surface of the waveguide for all these TE_{0n} ($m = 0$) modes is the H_z component, while the electric field lines are circular. Therefore these modes are usually referred to as circular electric modes. For a constant power in the wave, the H_z component decreases as the frequency increases and approaches zero at infinite frequency. Simultaneously the current density and conductor losses on the waveguide walls also decrease and approach zero. Because of this attractive feature, these modes have received considerable attention for long-distance propagation of energy, especially at millimeter-wave frequencies. Typically attenuations as low as 1.25 dB/km (2 dB/mi) have been attained [2]. This is to be compared with attenuations of 120 dB/km for WR-90 copper rectangular waveguides, and 3 dB/km at 0.85 μm, and less than 0.5 dB/km at 1.3 μm for fiberoptic cables.

Although the TE_{0n} modes are very attractive from the attenuation point of view, there are a number of problems associated with their excitation and retention. One of the problems is that the TE_{01} mode, which is the first of the TE_{0n} modes, is not the dominant mode. Therefore in order for this mode to be above its cutoff frequency and propagate in the waveguide, a number of other modes (such as the TE_{11}, TM_{01}, TE_{21}, and TM_{11}) with lower cutoff frequencies can also exist. Additional modes can also be present if the operating frequency is chosen well above the cutoff frequency of the TE_{01} mode in order to provide a margin of safety from being too close to its cutoff frequency.

To support the TE_{01} mode, the waveguide must be oversized and it can support a number of other modes. One of the problems faced with such a guide is how to excite the desired TE_{01} mode with sufficient purity and suppress the others. Another problem is how to prevent coupling between the TE_{01} mode and undesired modes. The presence of the undesired modes causes not only higher losses but also dispersion and attenuation distortion to the signal since each exhibits different phase velocities and attenuation. Irregularities in the inner geometry, surface, and direction (bends, nonuniform cross sections, etc.) of the waveguide are the main contributors to the coupling to the undesired modes. However, for the guide to be of any practical use, it must be able to sustain and propagate the desired TE_{01} and other TE_{0n} modes efficiently over bends of reasonable curvature. One technique that has been implemented to achieve this is to use mode conversion before entering the corner and another conversion when exiting to convert back to the desired TE_{0n} mode(s).

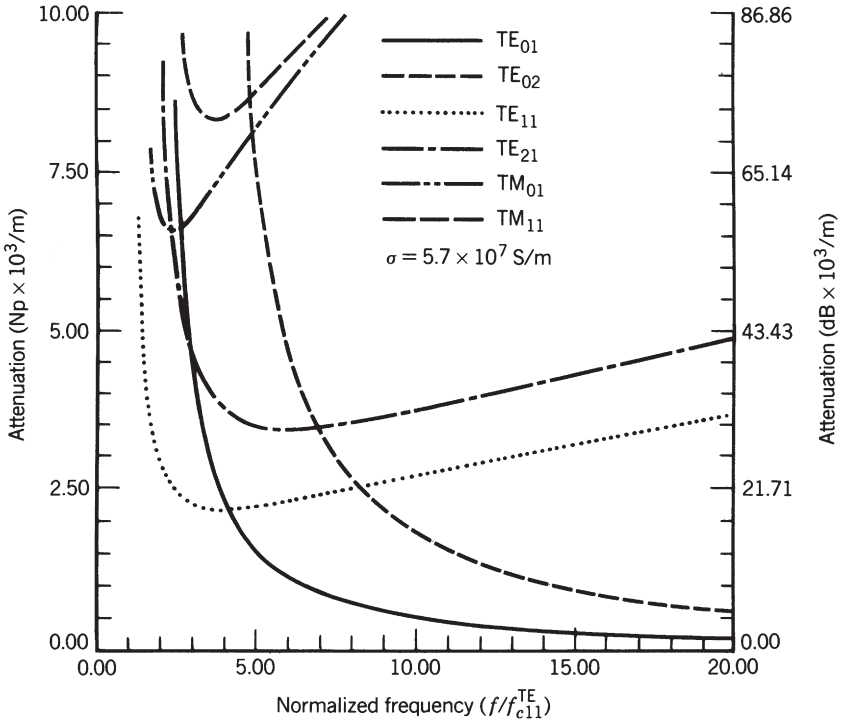

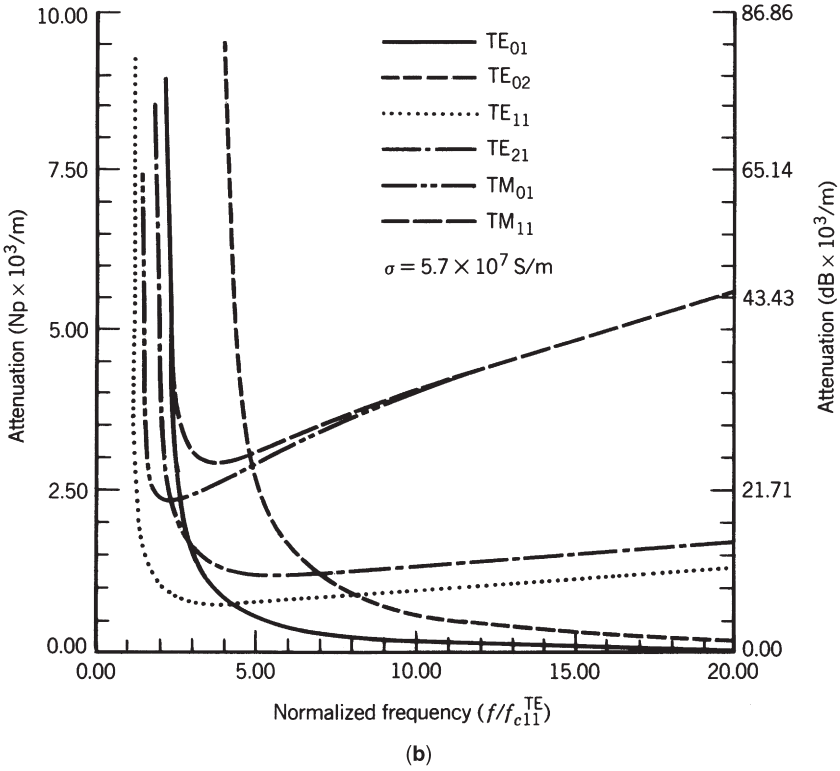

Figure 4. Attenuation for TE_{mn}^{z} and TM_{mn}^{z} modes in a circular waveguide: (a) $a = 1.5$ cm; (b) $a = 3$ cm.

Another method that has been used to discriminate against undesired modes and avoid coupling to them is to introduce filters inside the guide that cause negligible attenuation to the desired TE_{0n} mode(s). These filters introduce cuts that are perpendicular to the current paths of the undesired modes and parallel to the current direction of the desired mode(s). Since the current path of the undesired modes is along the axis (z direction) of the guide and the path of the desired TE_{0n} modes is along the circumference (ϕ direction), a helical wound wire placed on the inside surface of the guide can serve as a filter that discourages any mode that requires an axial

Table 3. Summary of TE^z_{mn} and TM^z_{mn} Mode Characteristics of Circular Waveguide

	$TE^z_{mn}\begin{pmatrix} m=0,1,2,\ldots, \\ n=1,2,3,\ldots \end{pmatrix}$	$TM^z_{mn}\begin{pmatrix} m=0,1,2,3,\ldots, \\ n=1,2,3,4,\ldots \end{pmatrix}$
E_ρ^+	$-A_{mn}\frac{m}{\varepsilon\rho}J_m(\beta_\rho\rho)[-C_2\sin(m\phi)+D_2\cos(m\phi)]e^{-j\beta_z z}$	$-B_{mn}\frac{\beta_\rho\beta_z}{\omega\mu\varepsilon}J'_m(\beta_\rho\rho)[C_2\cos(m\phi)+D_2\sin(m\phi)]e^{-j\beta_z z}$
E_ϕ^+	$A_{mn}\frac{\beta_\rho}{\varepsilon}J'_m(\beta_\rho\rho)[C_2\cos(m\phi)+D_2\sin(m\phi)]e^{-j\beta_z z}$	$-B_{mn}\frac{m\beta_z}{\omega\mu\varepsilon}\frac{1}{\rho}J_m(\beta_\rho\rho)[-C_2\sin(m\phi)+D_2\cos(m\phi)]e^{-j\beta_z z}$
E_z^+	0	$-jB_{mn}\frac{\beta_\rho^2}{\omega\mu\varepsilon}J_m(\beta_\rho\rho)[C_2\cos(m\phi)+D_2\sin(m\phi)]e^{-j\beta_z z}$
H_ρ^+	$-A_{mn}\frac{\beta_\rho\beta_z}{\omega\mu\varepsilon}J'_m(\beta_\rho\rho)[C_2\cos(m\phi)+D_2\sin(m\phi)]e^{-j\beta_z z}$	$B_{mn}\frac{m}{\mu}\frac{1}{\rho}J_m(\beta_\rho\rho)[-C_2\cos(m\phi)+D_2\sin(m\phi)]e^{-j\beta_z z}$
H_ϕ^+	$-A_{mn}\frac{m\beta_z}{\omega\mu\varepsilon}\frac{1}{\rho}J_m(\beta_\rho\rho)[-C_2\sin(m\phi)+D_2\cos(m\phi)]e^{-j\beta_z z}$	$-B_{mn}\frac{\beta_\rho}{\mu}J'_m(\beta_\rho\rho)[-C_2\cos(m\phi)+D_2\sin(m\phi)]e^{-j\beta_z z}$
H_z^+	$-jA_{mn}\frac{\beta_\rho^2}{\omega\mu\varepsilon}J_m(\beta_\rho\rho)[C_2\cos(m\phi)+D_2\sin(m\phi)]e^{-j\beta_z z}$	0
$\beta_c=\beta_\rho$	$\frac{\chi'_{mn}}{a}$	$\frac{\chi_{mn}}{a}$
f_c	$\frac{\chi'_{mn}}{2\pi a\sqrt{\mu\varepsilon}}$	$\frac{\chi_{mn}}{2\pi a\sqrt{\mu\varepsilon}}$
λ_c	$\frac{2\pi a}{\chi'_{mn}}$	$\frac{2\pi a}{\chi_{mn}}$
$\beta_z(f\geq f_c)$	$\beta\sqrt{1-\left(\frac{f_c}{f}\right)^2}=\beta\sqrt{1-\left(\frac{\lambda}{\lambda_c}\right)^2}$	
$\lambda_g(f\geq f_c)$	$\frac{\lambda}{\sqrt{1-\left(\frac{f_c}{f}\right)^2}}=\frac{\lambda}{\sqrt{1-\left(\frac{\lambda}{\lambda_c}\right)^2}}$	
$v_p(f\geq f_c)$	$\frac{v}{\sqrt{1-\left(\frac{f_c}{f}\right)^2}}=\frac{v}{\sqrt{1-\left(\frac{\lambda}{\lambda_c}\right)^2}}$	
$Z_w(f\geq f_c)$	$\frac{\eta}{\sqrt{1-\left(\frac{f_c}{f}\right)^2}}=\frac{\eta}{\sqrt{1-\left(\frac{\lambda}{\lambda_c}\right)^2}}$	$\eta\sqrt{1-\left(\frac{f_c}{f}\right)^2}=\eta\sqrt{1-\left(\frac{\lambda}{\lambda_c}\right)^2}$
$Z_w(f\leq f_c)$	$j\frac{\eta}{\sqrt{\left(\frac{f_c}{f}\right)^2-1}}=j\frac{\eta}{\sqrt{\left(\frac{\lambda}{\lambda_c}\right)^2-1}}$	$-j\eta\sqrt{\left(\frac{f_c}{f}\right)^2-1}=-j\eta\sqrt{\left(\frac{\lambda}{\lambda_c}\right)^2-1}$
α_c	$\frac{R_s}{a\eta\sqrt{1-\left(\frac{f_c}{f}\right)^2}}\left[\left(\frac{f_c}{f}\right)^2+\frac{m^2}{(\chi'_{mn})^2-m^2}\right]$	$\frac{R_s}{a\eta}\frac{1}{\sqrt{1-\left(\frac{f_c}{f}\right)^2}}$

component of current flow but propagates the desired TE_{0n} modes [3,4].

Another means to suppress undesired modes is to introduce within the guide very thin baffles of lossy material that will act as attenuating sheets. The surfaces of the baffles are placed in the radial direction of the guide so that they are parallel to the E_ρ and E_z components of the undesired modes (which will be damped) and normal to the E_ϕ component of the TE_{0n} modes that will remain unaffected. Typically two baffles are placed in a crossed pattern over the cross section of the guide.

A summary of the pertinent characteristics of the TE^z_{mn} and TM^z_{mn} modes of a circular waveguide are found listed in Table 3.

BIBLIOGRAPHY

1. C. S. Lee, S. W. Lee, and S. L. Chuang, Plot of modal field distribution in rectangular and circular waveguides, *IEEE Trans. Microwave Theory* Tech. **MTT-33**(3):271–274 (March 1985).
2. S. E. Miller, Waveguide as a communication medium, *Bell Syst. Tech. J.* **33**:1209–1265 (Nov. 1954).

3. S. P. Morgan and J. A. Young, Helix waveguide, *Bell Syst. Tech. J.* **35**:1347–1384 (Nov. 1956).
4. S. Ramo, J. R. Whinnery, and T. Van Duzer, *Fields and Waves in Communication Electronics*, Wiley, New York, 1965, pp. 429–439.

COAXIAL LINE DISCONTINUITIES

R. GARG
Indian Institute of Technology
Kharagpur
Kharagpur, India

Various types of coaxial-line discontinuities have been discussed in the literature [1–4], including: capacitive gaps, open-ended configuration, impedance steps, capacitive windows, T junctions, small elliptical and circular apertures, aperture coupling between two coaxial lines, and bifurcation of a coaxial line. The configurations and the equivalent circuits for some of the discontinuities are shown in Fig. 1. The mode-matching technique with variational formulation is the commonly used approach to arrive at the equivalent-circuit parameters of discontinuities. The available results for some of these discontinuities are summarized in the following sections.

1. CAPACITIVE GAPS IN COAXIAL LINES

A gap in the center conductor of a coaxial line, as shown in Fig. 1a, introduces mainly a series capacitance in the line. This type of discontinuity finds common use in microwave filters, DC blocks, and coaxial-line reentrant cavity.

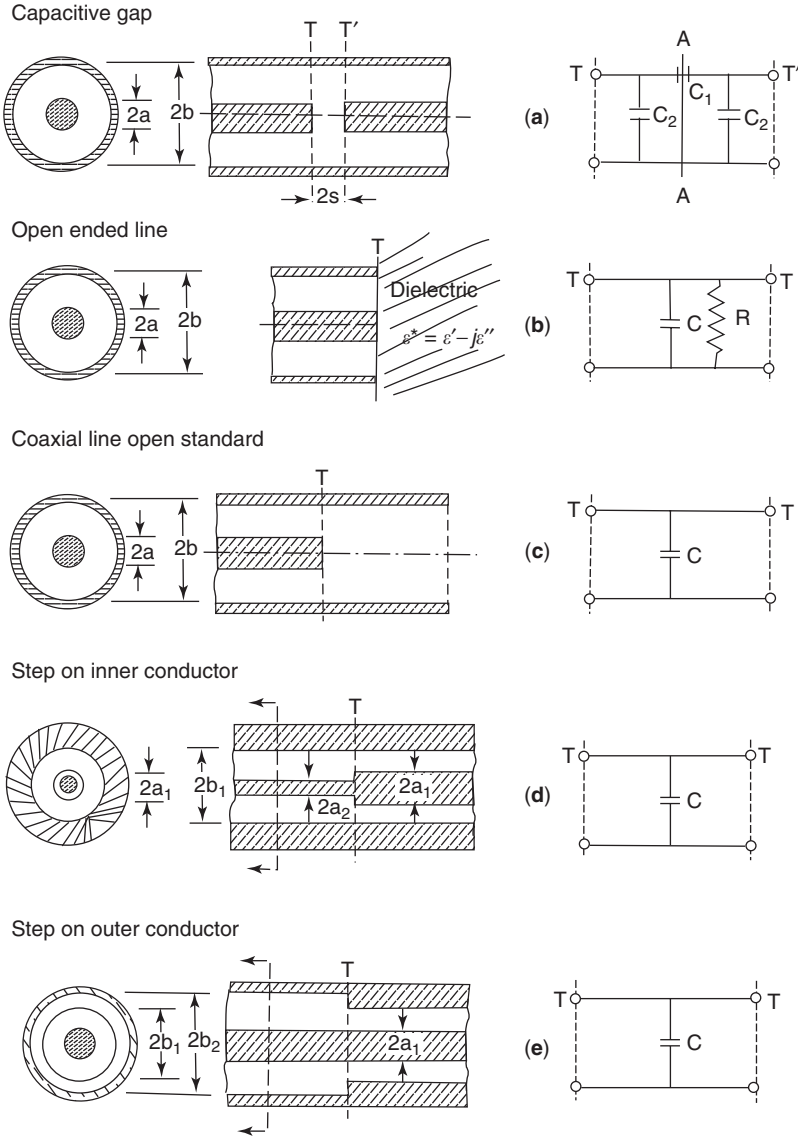

Figure 1. Discontinuities in coaxial lines and their equivalent circuits.